Article

Comparison of Performance of Micro-Computed Tomography (Micro-CT) and Synchrotron Radiation CT in Assessing Coronary Stenosis Caused by Calcified Plaques in Coronary Artery Phantoms

Curtise K. C. Ng [1,2,]*, Zhonghua Sun [1,2] and Shirley Jansen [1,3,4,5]

1   Curtin Medical School, Curtin University, GPO Box U1987, Perth, WA 6845, Australia;
    z.sun@curtin.edu.au (Z.S.); s.jansen@curtin.edu.au (S.J.)
2   Curtin Health Innovation Research Institute (CHIRI), Faculty of Health Sciences, Curtin University,
    GPO Box U1987, Perth, WA 6845, Australia
3   Department of Vascular Surgery, Sir Charles Gairdner Hospital, Hospital Avenue,
    Nedlands, WA 6009, Australia
4   Heart & Vascular Research Institute, Harry Perkins Medical Research Institute, 6 Verdun Street,
    Nedlands, WA 6009, Australia
5   Faculty of Health and Medical Sciences, The University of Western Australia, 35 Stirling Highway,
    Perth, WA 6009, Australia
*   Correspondence: curtise.ng@curtin.edu.au or curtise_ng@yahoo.com.hk; Tel.: +61-8-9266-7314;
    Fax: +61-8-9266-2377

Abstract: Synchrotron-radiation-computed tomography (SRCT) allows more accurate calcified plaque and coronary stenosis assessment as a result of its superior spatial resolution; however, typical micro-computed tomography (micro-CT) systems have even higher resolution. The purpose of this study was to compare the performance of high-resolution micro-CT with SRCT in the assessment of calcified plaques and a previously published dataset of coronary stenosis assessment. This experimental study involved micro-CT scanning of three-dimensional printed coronary artery models with calcification in situ used in our previously published SRCT study on coronary stenosis assessment. Measurements of coronary stenosis utilizing both modalities were compared using a paired sample *t*-test. The degrees of stenosis measured on all but one micro-CT dataset were statistically significantly lower than the corresponding SRCT measurements reported in our previous paper ($p < 0.0005$–0.05). This indicates that the superior spatial resolution of micro-CT was able to further reduce over-estimation of stenosis caused by extensive calcification of coronary arteries and, hence, false positive results. Our results showed that the high-resolution micro-CT used in this study outperformed the Australian Synchrotron SRCT in both calcified plaque and coronary stenosis assessment. These findings will become clinically important for cardiovascular event prediction and enable reclassification of individuals with low and intermediate risk into appropriate risk categories when the technical challenges of micro-CT in clinical practice such as the small field of view and demanding on image processing power are addressed.

Keywords: 3D printing; accuracy; calcification; cardiovascular disease; computed tomography; coronary artery disease; coronary stenosis; micro-computed tomography; plaque; synchrotron radiation

1. Introduction

Coronary computed tomography angiography (CCTA) is commonly used for coronary artery disease (CAD) diagnosis because it is a less-invasive imaging modality and performs well in coronary stenosis assessment and cardiac event prediction [1–3]. For low to intermediate coronary stenosis, CCTA has very high negative predictive value as a result of its ability to exclude significant stenosis [4]. Nonetheless, CCTA has high false positive results

in patients with extensive calcified plaques in the coronary arteries by causing blooming artifact, which exaggerates plaque size and, hence, affects diagnostic value. Previous studies showed that its specificity and positive predictive value (PPV) in calcification is only 18–53% [5,6]. According to the European Society of Cardiology (ESC)'s guidelines for the diagnosis and management of chronic coronary syndromes, CCTA is the preferred imaging modality in patients with a lower likelihood of CAD due to its high accuracy for the detection of obstructive coronary stenosis [7]. However, in the presence of extensive calcification, CCTA is not recommended because of increased possibility of non-diagnostic image quality affecting diagnostic value of CCTA in assessing calcified plaques.

Various approaches were investigated for improving CCTA performance in calcification such as the use of image post-processing and iterative reconstruction (IR) to reduce blooming artifact [6,8–10], inclusion of the left coronary bifurcation angle in analysis [11–13], and through use of thinner slices (230 μm high-resolution computed tomography (CT)) [14]. These methods addressed the limitations of CCTA in diagnosing calcified coronary plaques to some extent with improved specificity and PPV. Use of IR has become a routine practice with a variety of IR algorithms introduced into cardiac CT practice by multiple CT vendors [15]. Studies showed that use of IR significantly reduced both the calcium volume and score in comparison with the filtered back projection, leading to improved specificity and PPV [16–18]. Despite promising results, use of IR needs to be cautious as some studies reported contradictory findings with no significant impact on calcium volume changes when IR algorithms were applied to these CCTA images [19,20]. Use of image post-processing methods such as calcium subtraction as proposed by Tanaka et al. and sharpening method as indicated by our previous study improved sensitivity and PPV by up to 30% [6,8,21], but this was still insufficient, as the diagnostic value of CCTA was less than 70% in these studies. The use of left coronary angulation as an alternative to standard lumen assessment was shown to significantly increase the specificity and PPV (reaching 79% and 81%, respectively, on a per-vessel assessment) when assessing calcified plaques on CCTA [11–13]. The main limitation in measurement of left coronary angulation is due to lack of standard approach of whether two-dimensional (2D) axial or three-dimensional (3D) volume rendering views are used to determine the left coronary bifurcation angles. Furthermore, this approach does not address the fundamental issue of CCTA in diagnosing calcified plaques, as it only serves as an alternative to the standard approach of lumen measurement rather than solving the limitations. The improved spatial resolution of CCTA will represent an effective and feasible approach to solve this challenging issue. Pontone and colleagues in their randomized controlled trial compared high-resolution with standard CCTA (0.23 mm vs. 0.625 mm) in 184 patients with high risk of CAD [22]. High-resolution CCTA showed significantly higher specificity and PPV when compared to standard resolution CCTA on per-segment and per-patient analysis (98% and 92% vs. 95% and 80%; $p < 0.001$; 91% and 98% vs. 46% and 92%; $p < 0.01$, respectively). This highlights the significance of using high-resolution CT in CCTA, especially in patients with heavily calcified plaques.

However, spatial resolution of synchrotron-radiation-CT (SRCT, $19 \times 19 \times 19$ μm^3) is much higher than that of conventional CT [23], as demonstrated in our previous study [24]. Nonetheless, typical micro-CT systems have spatial resolutions as low as $0.5 \times 0.5 \times 0.5$ μm^3, which are far better than that of SRCT and, hence, should improve diagnostic performance of calcified plaque evaluation [24,25]. To the best of our knowledge, no study has been conducted to compare the performance of these two imaging modalities in the assessment of coronary arterial lumen loss and calcification. The purpose of this study was to compare the performance of high-resolution micro-CT with the SRCT in the calcified plaques and coronary stenosis assessment. We hypothesized that the superior resolution of micro-CT allowed for an improvement in assessment of coronary stenosis in the presence of calcified plaques.

2. Materials and Methods

We used previously developed 3D-printed coronary models with simulation of calcified plaques to explore the hypothesis given the long scanning time of micro-CT and the limited field of view [24,26]. The 3D-printed heart and vascular models derived from CT or magnetic resonance images can replicate anatomical structures and pathologies with a high degree of accuracy, thus serving as a useful tool for understanding complex cardiac anatomy and simulating surgical or interventional procedures [27–34]. Our models were created based on CCTA datasets of three patients with different degrees of coronary artery stenosis caused by calcified plaques. A Stratasys Objet500 Connex3 multi-material (Poly-jet) 3D printer (Objective 3D, Melbourne, Victoria, Australia) was used to print coronary artery walls and calcifications with TangoPlus (83 Hounsfield unit (HU)) and VeroWhite (136 HU) materials, respectively [35]. These printing materials were chosen because their attenuation properties matched those of the corresponding structures, which were around 89 HU (artery wall) and at least 130 HU (calcified plaque) [36–38]. A summary of the anatomical characteristics of these three models is shown below. Further details of the CCTA datasets, patients, and 3D printing involved in this experimental study were given in our previous publication [24]. Ethical approval was not required in this study, as only 3D-printed coronary artery models were used (Figure 1).

- Model 1: >90% and <50% stenosis in left main stem (LM) and left anterior descending (LAD) coronary artery, respectively.
- Model 2: >90% and 70% stenosis in LAD and left circumflex (LCx), respectively.
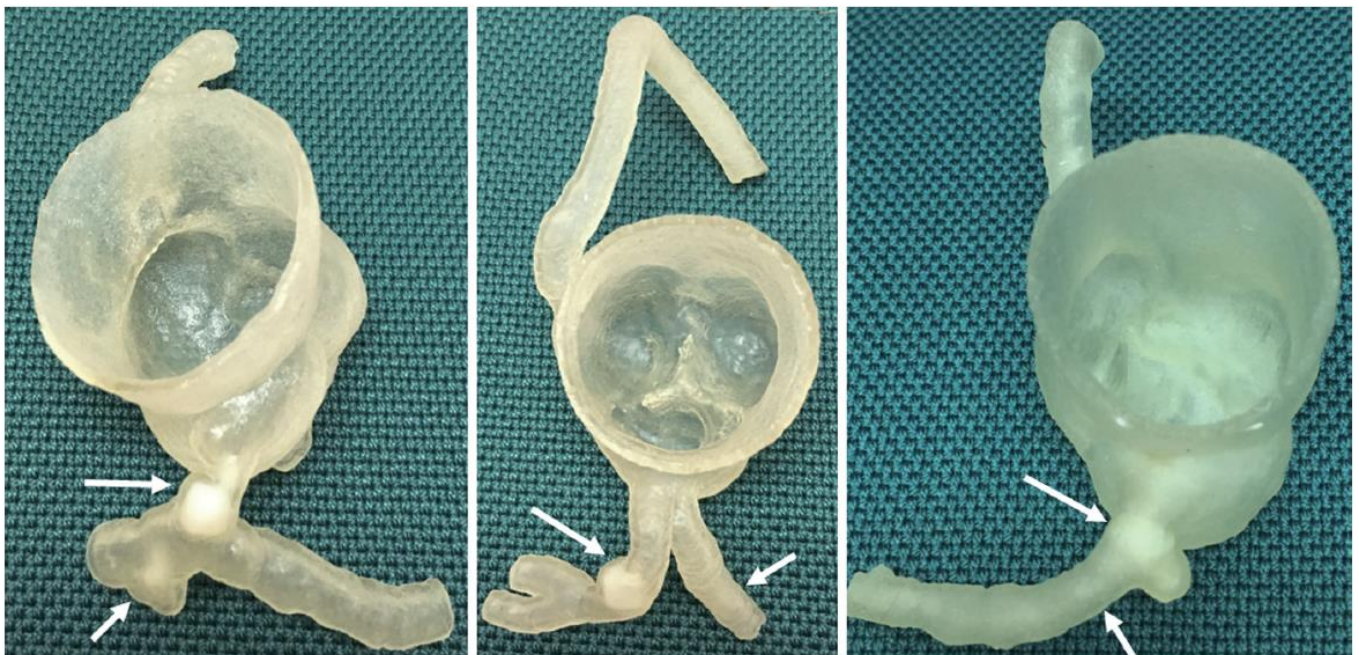- Model 3: >90% and 70% stenosis in proximal LCx and middle LCx, respectively.

Figure 1. Three-dimensional-printed coronary models with simulation of calcified plaques (arrows) in the left coronary arteries. Reprint from Sun et al. [24] with permission.

Skyscan 1176 micro-CT system (Bruker Corporation, Billerica, MA, USA) available at Australian National Imaging Facility in Centre for Microscopy, Characterisation, and Analysis (CMCA) at Harry Perkins Institute of Medical Research was used to scan the three models at its highest spatial resolution ($8.7 \times 8.7 \times 8.7 \ \mu m^3$) and lowest tube voltage (40 kV) settings. The selection of the lowest tube voltage was based on our previous SRCT findings that a lower beam energy (30 keV) provided better visualization of coronary artery walls and calcified plaques as a result of the materials used: TangoPlus and VeroWhite, which had low X-ray attenuation properties [24,39–42]. Figure 2 shows the micro-CT scan setup.
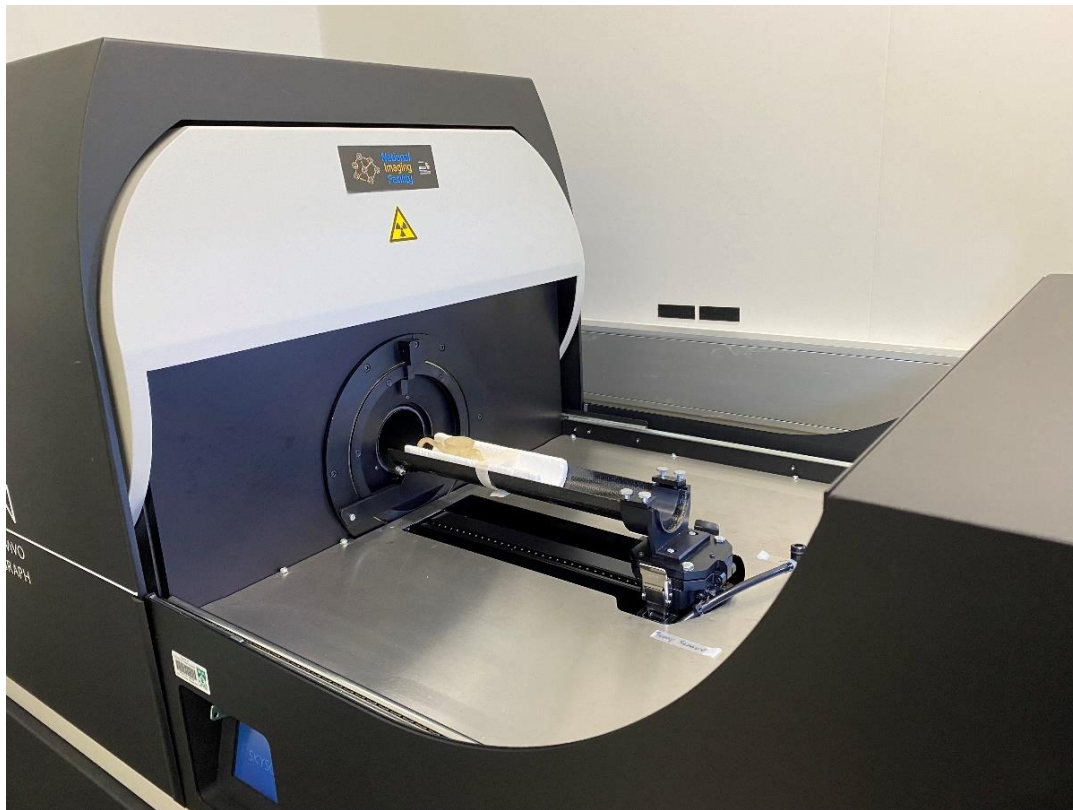
Figure 2. Micro-computed tomography scan with model 2 placed on the scan table.

Axial micro-CT images of the three models in tagged image file format (TIFF) were converted to Analyze 7.5 file format by the open-source image processing program ImageJ (v1.52a, National Institutes of Health, Bethesda, MD, USA) for importing into the Analyze 12 software package (AnalyzeDirect, Inc., Lexana, KS, USA) with multi-dimensional image display, processing, and measurement capabilities on an image processing workstation (Hewlett-Packard Z4 G4 (Palo Alto, CA, USA) with Intel Xeon W-2255 3.7 GHz central processing unit (Santa Clara, CA, USA), 512 GB random access memory and Nvidia RTX A6000 48 GB graphics processing unit (Santa Clara, CA, USA)). The degree of coronary lumen stenosis was measured on 2D axial images of the three models by one observer with more than 20 years of CCTA image interpretation experience. Three measurements were performed for each stenotic area with their average value used as the final value, to minimize intra-observer variation. Intra-observer agreement was determined by randomly selecting images of each model and repeating the measurements by the same observer after two weeks. Good intra-observer reliability between these measurements was found ($r = 0.835$, $p < 0.01$). Details of the measurement approach were given in our previous reports [40,41,43–45].

SPSS Statistics 28 (International Business Machines Corporation, Armonk, NY, USA) was used for statistical analysis. Mean and standard deviation were calculated for continuous variables. The measurements of coronary lumen stenosis on the micro-CT images of the three models were compared with the corresponding measurements performed on SRCT acquired with a beam energy of 30 keV reported previously using a paired sample *t*-test to determine the modality able to provide better coronary stenosis assessment [24]. A *p*-value less than 0.05 represented statistical significance.

3. Results

Tables 1 and 2 show the micro-CT stenosis assessment performances for all six plaques in the three 3D-printed coronary artery models. The degrees of stenosis measured on

the micro-CT images of the models (except the one caused by plaque 2 in model 3) were statistically significantly lower than the corresponding SRCT measurements reported in our previous paper ($p < 0.0005$–0.05) [24]. This indicates that the superior spatial resolution of micro-CT was able to further suppress the blooming artifact caused by the extensive calcification. Nonetheless, the degrees of stenosis measured on the micro-CT images of plaques 1 and 2 of models 1 and 2 were lower than the ground truths (degrees of stenosis calculated based on the true sizes of simulated plaques and models).

Table 1. Comparison of micro-computed tomography (micro-CT) and synchrotron-radiation-CT (SRCT) performance in measuring left coronary stenosis in plaque 1 > 90% stenosis [24].

| Model | Degree of Lumen Stenosis (%) | | | | | *p*-Value |
| | Micro CT | SRCT | | | | |
	0.009 mm ST	0.095 mm ST	0.208 mm ST	0.302 mm ST	0.491 mm ST	
1	86.2 ± 0.033	99.1 ± 0.004	98.8 ± 0.003	99.1 ± 0.004	100 ± 0.000	<0.005
2	80.0 ± 0.044	97.2 ± 0.025	97.8 ± 0.022	96.4 ± 0.012	96.4 ± 0.010	<0.0005
3	94.4 ± 0.000	99.2 ± 0.005	97.2 ± 0.009	97.8 ± 0.005	100 ± 0.000	<0.0005

CT, computed tomography; ST, slice thickness.

Table 2. Comparison of micro-computed tomography (micro-CT) and synchrotron-radiation-CT (SRCT) performance in measuring left coronary stenosis in plaque 2: <50% stenosis (model 1), and 70% stenosis (models 2 and 3) [24].

| Model | Degree of Lumen Stenosis (%) | | | | | *p*-Value |
| | Micro CT | SRCT | | | | |
	0.009 mm ST	0.095 mm ST	0.208 mm ST	0.302 mm ST	0.491 mm ST	
1	46.4 ± 0.035	47.4 ± 0.007	47.3 ± 0.001	48.6 ± 0.022	55.1 ± 0.036	<0.05
2	60.0 ± 0.031	70.0 ± 0.003	71.7 ± 0.022	77.8 ± 0.011	84.8 ± 0.008	<0.0005
3	75.0 ± 0.000	71.5 ± 0.011	75.2 ± 0.017	74.7 ± 0.021	85.1 ± 0.078	0.091

CT, computed tomography; ST, slice thickness.

Figures 3–8 show the micro-CT and SRCT images of plaques 1 and 2 in models 1–3 that were used for the stenosis assessments. For the micro-CT (0.009 mm slice thickness) images, only the stenotic areas were illustrated due to the processing power limit of the workstation for handling data with a very large matrix (7872 × 7872). The micro-CT (0.009 mm slice thickness) images were able to clearly demonstrate patent areas between the calcification and the left coronary arterial walls, especially in severe stenosis compared with SRCT (0.095–0.491 mm slice thickness) images (Figures 3–5 with >90% stenosis).
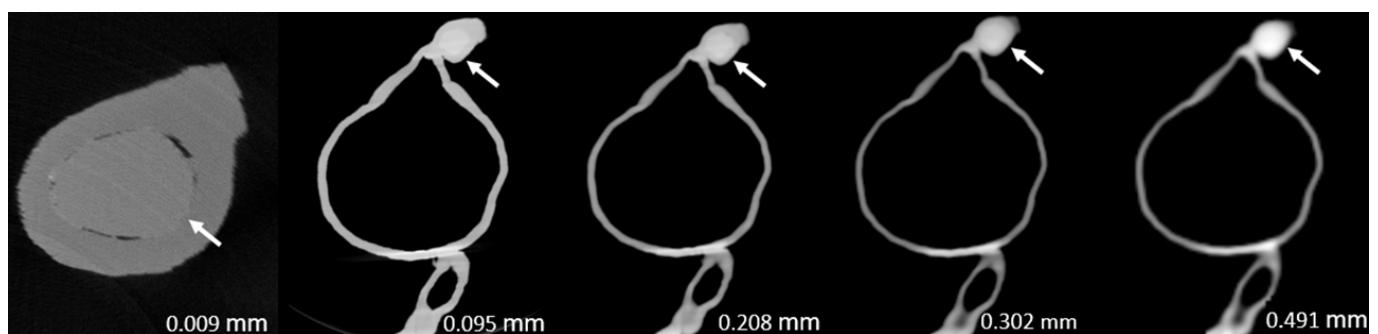

Figure 3. Two-dimensional micro-computed tomography (micro-CT) (0.009 mm slice thickness) and synchrotron-radiation-CT (0.095–0.491 mm slice thickness) images of plaque 1 (arrow) in model 1 causing >90% stenosis (reprint of synchrotron-radiation-CT images with permission [24]).
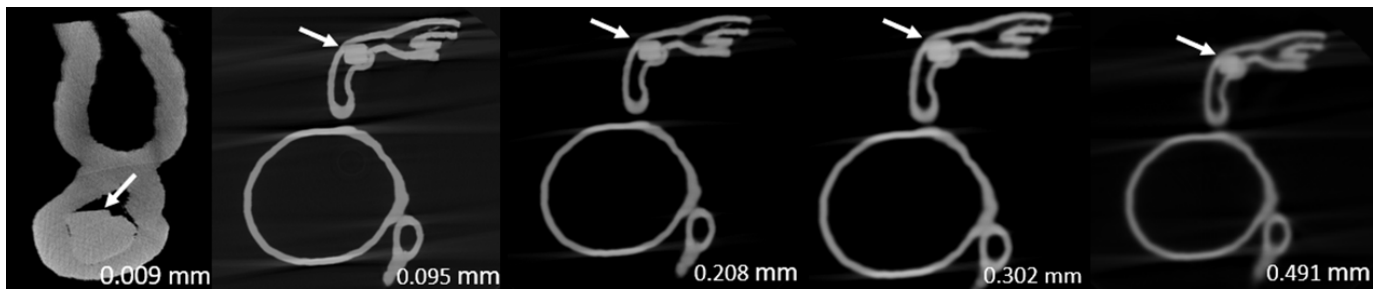
Figure 4. Two-dimensional micro-computed tomography (micro-CT) (0.009 mm slice thickness) and synchrotron-radiation-CT (0.095–0.491 mm slice thickness) images of plaque 1 (arrow) in model 2 causing >90% stenosis (reprint of synchrotron-radiation-CT images with permission [24]).
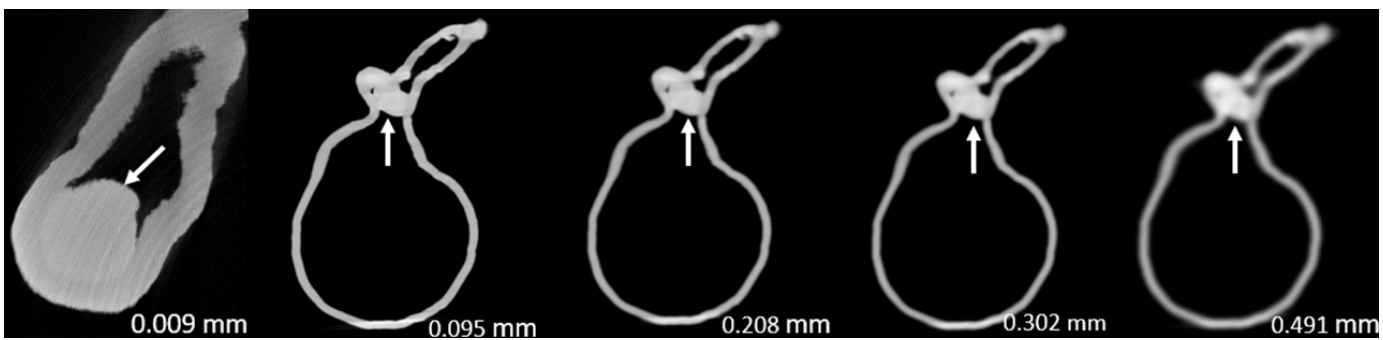
Figure 5. Two-dimensional micro-computed tomography (micro-CT) (0.009 mm slice thickness) and synchrotron-radiation-CT (0.095–0.491 mm slice thickness) images of plaque 1 (arrow) in model 3 causing >90% stenosis (reprint of synchrotron-radiation-CT images with permission [24]).
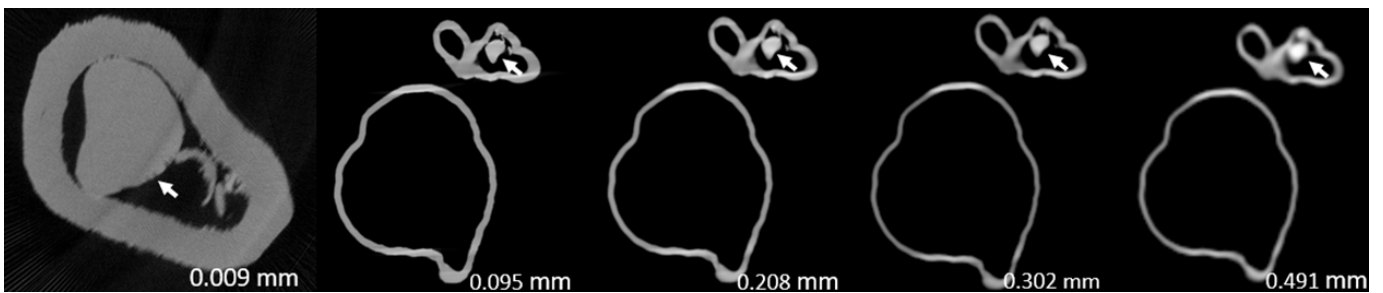
Figure 6. Two-dimensional micro-computed tomography (micro-CT) (0.009 mm slice thickness) and synchrotron-radiation-CT (0.095–0.491 mm slice thickness) images of plaque 2 (arrow) in model 1 causing <50% stenosis (reprint of synchrotron-radiation-CT images with permission [24]).
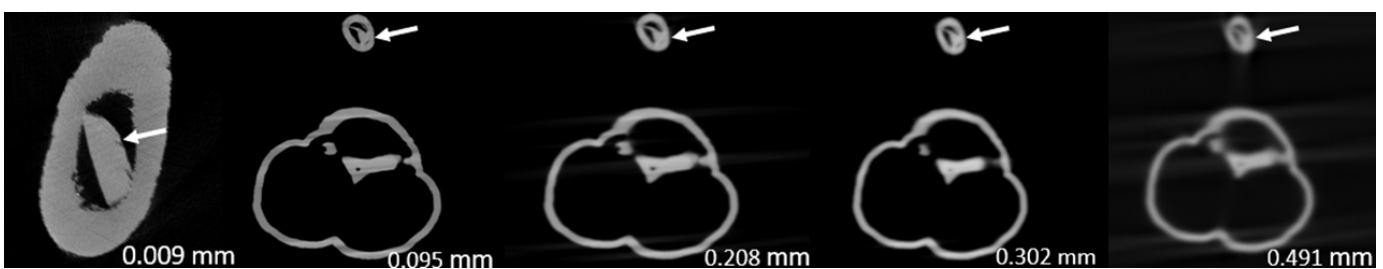
Figure 7. Two-dimensional micro-computed tomography (micro-CT) (0.009 mm slice thickness) and synchrotron-radiation-CT (0.095–0.491 mm slice thickness) images of plaque 2 (arrow) in model 2 causing 70% stenosis (reprint of synchrotron-radiation-CT images with permission [24]).

Figure 8. Two-dimensional micro-computed tomography (micro-CT) (0.009 mm slice thickness) and synchrotron-radiation-CT (0.095–0.491 mm slice thickness) images of plaque 2 (arrow) in model 3 causing 70% stenosis (reprint of synchrotron-radiation-CT images with permission [24]).
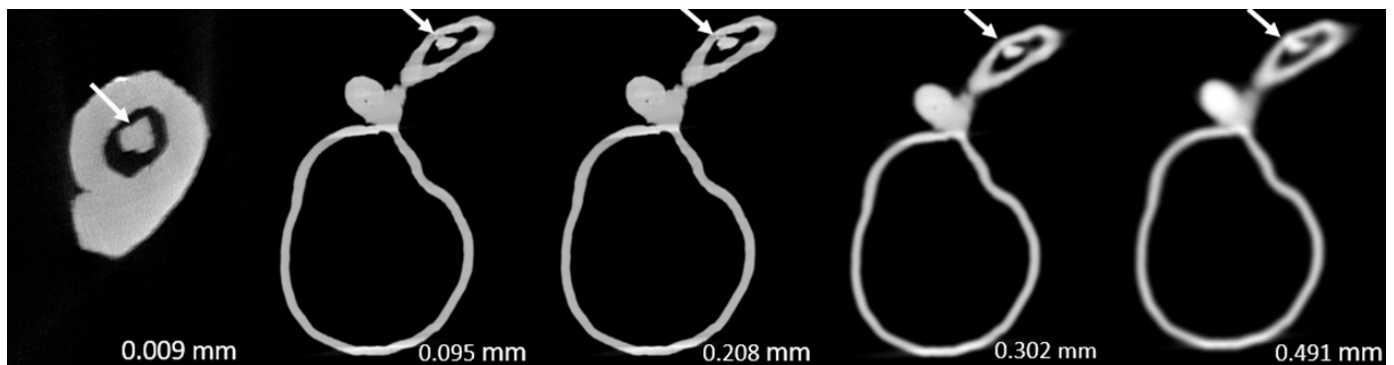
4. Discussion

To the best of our knowledge, this is the first study to compare the performance of high-resolution micro-CT with SRCT in calcified plaque and coronary stenosis assessment. Our findings show that the superior resolution of micro-CT allows for statistically significant improvements ($p < 0.0005$–0.05) in the assessment of stenosis in the presence of calcified plaques (except plaque 2 within model 3) with regard to blooming artifact suppression, hence minimizing over-estimation when compared with the corresponding results of our previous SRCT study [24]. This potentially reduces the false positive rate and improves specificity and PPV, if the micro-CT is applied to clinical practice for addressing the well-known weakness of the CCTA in the assessment of coronary stenosis with extensive calcification [5,6,46,47].

Although micro-CT seemed to outperform SRCT for blooming artifact suppression, Tables 1 and 2 reveal that the degree of stenosis measured on the micro-CT images of plaques 1 and 2 of models 1 and 2 were obviously lower than the ground truths, representing under-estimation of the stenoses. Similar findings were also noted in the results of our previous study, where higher SRCT beam energies such as 50 keV were able to further reduce blooming artifact but affected visualization of coronary artery walls and calcified plaques [24]. The use of a higher beam energy (tube potential) is one of the well-known strategies to suppress blooming artifact because the calcified plaque is a high-density material that can easily attenuate radiation with lower energies [42]. However, a higher tube potential was deemed unsuitable for soft tissue visualization such as coronary arteries because its density was lower than that of the calcification. Unfortunately, the lowest tube potential available on the Skyscan 1176 micro-CT scanner was 40 kV.

Another issue of micro-CT was its small field of view (FOV). As shown in Figure 1, the scan table was just large enough to accommodate the 3D-printed coronary artery models and, therefore, not applicable for clinical use. However, micro-CT scanners with greater FOVs such as 43.2×43.2 cm^2 have become available more recently [48]. This may make it possible to manufacture a clinical CT scanner with superior spatial resolution matching micro-CT performance in the future. Nevertheless, it is still a challenge for current image processing workstations to handle high-resolution CT images with large matrix size. For example, each model dataset in this study had around 10,000 images with 7872×7872 pixels and bit depth of 16 (2 bytes), and hence, every dataset size was about 1 TB (7872×7872 pixels $\times$ 2 bytes $\times$ 10,000 images). Additionally, the long scanning time of micro-CT needs to be addressed, and so, it may take some years for micro-CT technology to be applied in clinical practice. This would be similar to the previous CT system development that took decades for implementing iterative reconstruction into clinical practice since its emergence in 1970s due to the previous processing power limit of computers which also affected its scanning time and spatial resolution improvements [49–51].

When the aforementioned issues of micro-CT are addressed, it will be useful for cardiovascular event prediction by reclassifying individuals with low and intermediate risk categories to the appropriate risk categories and, therefore, safer clinical management along a spectrum where high-risk individuals often undergo interventional treatment, whereas low risk are usually followed up without any need for treatment [52,53]. If the use of micro-CT is combined with other blooming artifact suppression approaches such as the latest deep learning image reconstruction strategy, this may enable CT to become the imaging modality with a diagnostic performance matching the current gold standard of invasive coronary angiography. This has significant implications for interventional risks, radiation, and healthcare costs [9,10].

Although it is currently impossible to use micro-CT in patient imaging, the findings of this study highlight the importance of using high-resolution imaging for the improvement of assessing calcified coronary plaques and a reduction in false positive rates. Compared to the current medical CT scanners with $0.5 \times 0.5 \times 0.5$ mm spatial resolution, photon-counting CT represents the latest technological advancement with ultra-high-resolution of 0.2 mm, excellent image quality, and a further reduction in blooming artifact caused by the severe calcification or coronary stents [54–58]. Recent studies based on phantom experiments showed that photon-counting CT improved quantification of coronary stenosis with reduced blooming artifact, independent of heart rates when compared to the standard CCTA (0.2 mm vs. 0.4 mm slice thickness) [54,55]. This was also confirmed by patient studies using the photon-counting CT. Si-Mohamed et al. reported their initial experience with photon-counting CT in patients with 100% improvement in overall image quality in calcification [56]. Hagar et al. analyzed imaging of 68 patients showing that photon-counting CT had 96% sensitivity, 84% specificity, and 88% accuracy in the assessment of significant CAD. Even in patients with severe calcification (Agatston score of at least 1000), photon-counting CT still had a high performance with 93% sensitivity, 70% specificity, and 83% accuracy [57]. Soschynski et al., in their multi-center study consisting of 92 patients, further validated these findings with a high diagnostic performance: 92% sensitivity, 96% specificity, and 95% accuracy (Figure 9) [58]. Photon-counting CT is likely to make significant contributions to the improvement of diagnostic assessment of calcified coronary plaques in future.

This study had several limitations. Only one tube potential and one slice thickness were used for the micro-CT image acquisition. A comparison of high-resolution micro-CT with use of different resolutions such as 0.1–0.4 mm deserves to be investigated, as this is close to the CT resolution available in clinical practice. There were no thoracic structures surrounding the coronary models, and contrast medium was not used. However, these should not affect the assessment of calcified plaques and coronary stenosis, as evident in Figures 3–8, that the margins of vessel walls and plaques demonstrated on the micro-CT images were as sharp as those on the SRCT images or even better [24]. Although plaques of differing degree and location were simulated, only six were present in this study and clinical variation of arterial diameter, degree of disease, and location and number of plaques is wider. Most importantly, plaques can still be heterogeneous even when calcified, and this has implications on interpretation of detailed images [26].
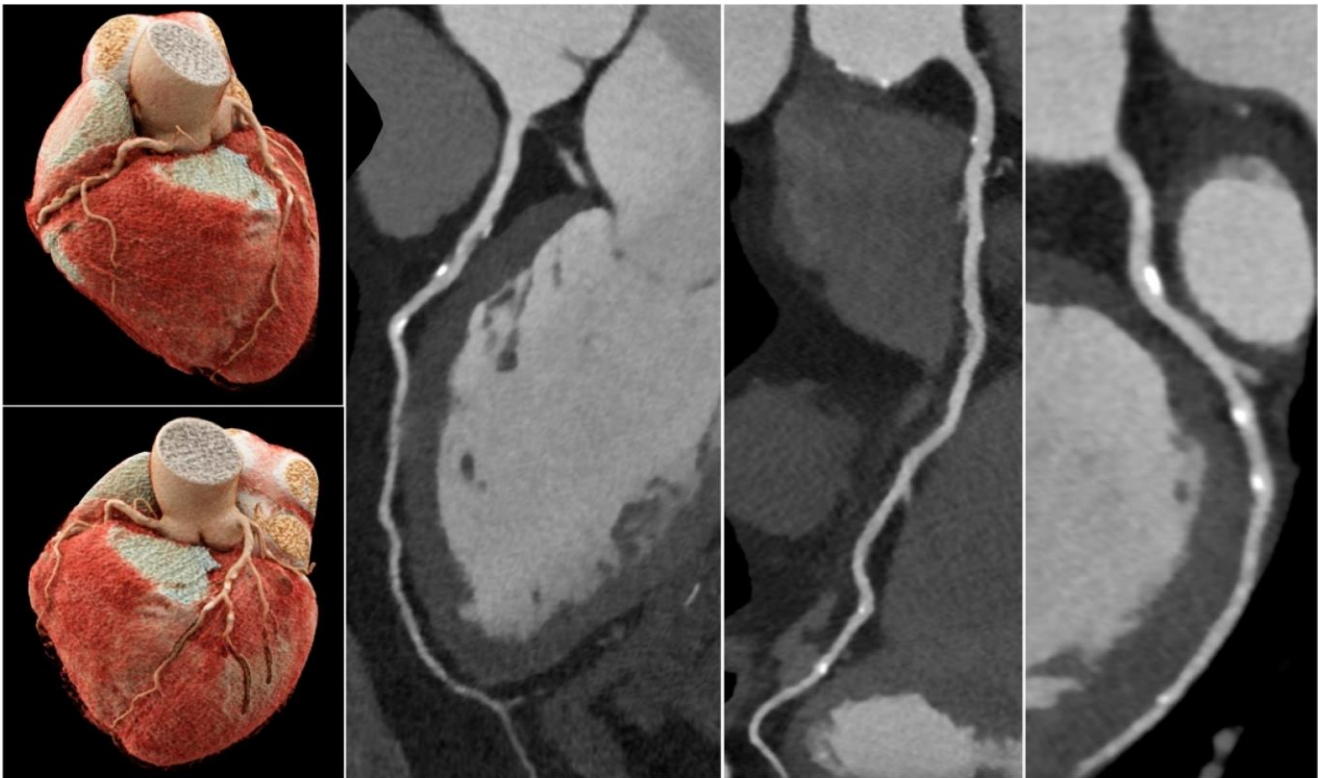
Figure 9. Coronary computed tomography angiography images of a 75-year-old male patient with atypical angina pectoris. Total Agatston score was 589. All coronary segments were diagnostic. Despite a high plaque burden, all calcified plaques were assessable with <50% stenosis and, hence, significant coronary stenosis could be excluded with high certainty. Reprinted from Soschynski et al. with permission under open access Creative Commons CC BY 4.0 license [58].

5. Future Directions and Perspectives

This study's findings suggest the future directions in improving diagnostic value of CCTA in assessing calcified plaques with a focus on improving spatial resolution as a practical approach from clinical perspectives. Although a variety of strategies have been proposed in the literature to address the limitation of CCTA in the diagnosis of extensive calcification in coronary arteries, the results were not so promising, due to use of different approaches from different studies, lack of standardized methodology, or unsatisfactory results to achieve a high diagnostic value of CCTA [6,8,16–22]. CT resolution significantly improved since the introduction of multislice CT in clinical practice more than 20 years ago. With current CT scanners, the spatial resolution is between 0.5 mm and 0.625 mm, with 0.2 mm available with the latest CT model of photon-counting CT [54–58]. Therefore, CT spatial resolution reached the same level as that of invasive coronary angiography (0.2 mm), allowing it to provide accurate assessment of coronary artery and its branches, regardless of the diameter of coronary artery segments. With further improvement in spatial resolution, as shown in this study's results, diagnostic performance of CCTA in calcified plaques will be further enhanced, making it a reliable less-invasive modality in cardiac imaging practice.

Another research direction of CCTA in CAD including calcified plaques is the use of combination of anatomic and functional approaches to determine ischemic coronary lesions. CT-derived fractional flow reserve (CT-FFR) has been increasingly reported in the literature with increased specificity over standard anatomic assessment with CCTA alone. Single-center and randomized controlled trials have proved incremental value of CT-FFR over CCTA in guiding patient management, playing an important role in clinical decision-making and use of resources by avoiding unnecessary downstream examinations [59–61]. Gao et al., in their recent study, reported that CT-FFR had high specificity and PPV when

compared to the CCTA (84% and 82% vs. 54% and 61%), while CT perfusion-FFR showed better results, even in the presence of high calcium scores (total Agatston score on per-vessel: ≥400) with specificity and PPV being 93% and 89% [62]. Thus, the use of high-resolution CCTA-FFR will further augment the performance of CCTA in calcified plaques and this could make CCTA a more effective and reliable diagnostic method in patients with CAD.

6. Conclusions

Our results showed that the high-resolution micro-CT used in this study outperformed the Australian Synchrotron SRCT in calcified plaques and coronary stenosis assessment with regard to blooming artifact reduction. This highlights the importance of using high-resolution imaging for the improvement of assessing calcified coronary plaques and a reduction in false positive rates. This study's findings will become clinically important for cardiovascular risk prediction and allow reclassification of individuals with low and intermediate risk into the appropriate risk categories when the technical challenges of using micro-CT in clinical practice, such as small FOV and highly demanding image processing power, are addressed. Potentially, this will lead to optimal clinical management according to accurate risk prediction in a disease process where intervention carries risks and minimization of unnecessary coronary angiography and treatment must be paramount.

References

1. Sun, Z.; Lin, C. Diagnostic value of 320-slice coronary CT angiography in coronary artery disease: A systematic review and meta-analysis. *Curr. Med. Imaging* **2014**, *10*, 272–280. [CrossRef]
2. Xu, L.; Sun, Z.; Fan, Z. Non-invasive physiologic assessment of coronary stenoses using cardiac CT. *Biomed. Res. Int.* **2014**, *2014*, 435737. [CrossRef]
3. Sun, Z.; Choo, G.H.; Ng, K.H. Coronary CT angiography: Current status and continuing challenges. *Br. J. Radiol.* **2012**, *85*, 495–510. [CrossRef] [PubMed]
4. Lee, S.P.; Jang, E.J.; Kim, Y.J.; Cha, M.J.; Park, S.Y.; Song, H.J.; Choi, J.E.; Shim, J.I.; Ahn, J.; Lee, H.J. Cost-effectiveness of coronary CT angiography in patients with chest pain: Comparison with myocardial single photon emission tomography. *J. Cardiovasc. Comput. Tomogr.* **2015**, *9*, 428–437. [CrossRef]
5. Park, M.J.; Jung, J.I.; Choi, Y.S.; Ann, S.H.; Youn, H.J.; Jeeon, G.N.; Choi, H.C. Coronary CT angiography in patients with high calcium score: Evaluation of plaque characteristics and diagnostic accuracy. *Int. J. Cardiovasc. Imaging* **2011**, *27*, 43–51. [CrossRef]
6. Sun, Z.; Ng, C.K.C. High calcium scores in coronary CT angiography: Effects of image post-processing on visualization and measurement of coronary lumen diameter. *J. Med. Imaging Health Inf.* **2015**, *5*, 110–116. [CrossRef]
7. Knuuti, J.; Wijns, W.; Saraste, A.; Capodanno, D.; Barbato, E.; Funck-Brentano, C.; Prescott, E.; Storey, R.F.; Deaton, C.; Cuisset, T.; et al. ESC Scientific Document Group. 2019 ESC guidelines for the diagnosis and management of chronic coronary syndromes. *Eur. Heart J.* **2020**, *41*, 407–477. [CrossRef]
8. Sun, Z.; Ng, C.K.C.; Xu, L.; Fan, Z.; Lei, J. Coronary CT angiography in heavily calcified coronary arteries: Improvement of coronary lumen visualization and coronary stenosis assessment with image postprocessing methods. *Medicine* **2015**, *94*, e2148. [CrossRef] [PubMed]
9. Sun, Z.; Ng, C.K.C. Artificial intelligence (enhanced super-resolution generative adversarial network) for calcium deblooming in coronary computed tomography angiography: A feasibility study. *Diagnostics* **2022**, *12*, 991. [CrossRef]

10. Sun, Z.; Ng, C.K.C. Finetuned super-resolution generative adversarial network (artificial intelligence) model for calcium deblooming in coronary computed tomography angiography. *J. Pers. Med.* **2022**, *12*, 1354. [CrossRef]
11. Sun, Z.; Xu, L.; Fan, Z. Coronary CT angiography in calcified coronary plaques: Comparison of diagnostic accuracy between bifurcation angle measurement and coronary lumen assessment for diagnosing significant coronary stenosis. *Int. J. Cardiol.* **2016**, *203*, 78–86. [CrossRef]
12. Sun, Z. Coronary CT angiography in coronary artery disease: Correlation between virtual intravascular endoscopic appearances and left bifurcation angulation and coronary plaques. *Biomed. Res. Int.* **2013**, *2013*, 732059. [CrossRef] [PubMed]
13. Xu, L.; Sun, Z. Coronary CT angiography evaluation of calcified coronary plaques by measurement of left coronary bifurcation angle. *Int. J. Cardiol.* **2015**, *182*, 229–231. [CrossRef] [PubMed]
14. Andreini, D.; Pontone, G.; Mushtaq, S.; Conte, E.; Perchinunno, M.; Guglielmo, M.; Volpato, V.; Annoni, A.; Baggiano, A.; Formenti, A.; et al. Atrial fibrillation: Diagnostic accuracy of coronary CT angiography performed with a whole-heart 230-μm spatial resolution CT scanner. *Radiology.* **2017**, *284*, 676–684. [CrossRef] [PubMed]
15. Naoum, C.; Blanke, P.; Leipsic, J. Iterative reconstruction in cardiac CT. *J. Cardiovasc. Comput. Tomogr.* **2015**, *9*, 255–263. [CrossRef]
16. Shen, J.; Du, X.; Guo, D.; Cao, L.; Gao, Y.; Bai, M.; Li, P.; Liu, J.; Li, K. Noise-based tube current reduction method with iterative reconstruction for reduction of radiation exposure in coronary CT angiography. *Eur. J. Radiol.* **2013**, *82*, 349–355. [CrossRef]
17. Yin, W.H.; Lu, B.; Gao, J.B.; Li, P.L.; Sun, K.; Wu, Z.F.; Yang, W.J.; Zhang, X.Q.; Zheng, M.W.; McQuiston, A.D.; et al. Effect of reduced x-ray tube voltage, low iodine concentration contrast medium, and sonogram-affirmed iterative reconstruction on image quality and radiation dose at coronary CT angiography: Results of the prospective multicentre REALISE trial. *J. Cardiovasc. Comput. Tomogr.* **2015**, *9*, 215–224. [CrossRef] [PubMed]
18. Funabashi, N.; Irie, R.; Aiba, M.; Morimoto, R.; Kabashima, T.; Fujii, S.; Uehara, M.; Ozawa, K.; Takaoka, H.; Kobayashi, Y. Adaptive-iterative-dosereduction 3D with multisector-reconstruction method in 320-slice CT may maintain accurate-measurement of the Agatston-calcium-score of severe-calcification even at higher pulsating-beats and low tube-current in vitro. *Int. J. Cardiol.* **2013**, *168*, 601–603. [CrossRef]
19. van Osch, J.A.C.; Mouden, M.; van Dalen, J.A.; Timmer, J.R.; Reiffers, S.; Knollema, S.; Greuter, M.W.; Ottervanger, J.P.; Jager, P.L. Influence of iterative image reconstruction on CT-based calcium score measurements. *Int. J. Cardiovasc. Imaging* **2014**, *30*, 961–967. [CrossRef]
20. Renker, M.; Nance, J.W., Jr.; Schoepf, U.J.; O'Brien, T.X.; Zwerner, P.L.; Meyer, M.; Kerl, J.M.; Bauer, R.W.; Fink, C.F.; Vogl, T.J.; et al. Evaluation of heavily calcified vessel with coronary CT angiography: Comparison of iterative and filtered back projection image reconstruction. *Radiology* **2011**, *260*, 390–399. [CrossRef]
21. Tanaka, R.; Yoshioka, K.; Muranaka, K.; Chiba, T.; Ueda, T.; Sasaki, T.; Fusazaki, T.; Ehara, S. Improved evaluation of calcified segments on coronary CT angiography: A feasibility study of coronary calcium subtraction. *Int. J. Cardiovasc. Imaging* **2013**, *29*, 75–81. [CrossRef] [PubMed]
22. Pontone, G.; Bertella, E.; Mushtaq, S.; Loguercio, M.; Cortinovis, S.; Baggiano, A.; Conte, E.; Annoni, A.; Formenti, A.; Beltrama, V.; et al. Coronary artery disease: Diagnostic accuracy of CT coronary angiography-A comparison of high and standard spatial resolution scanning. *Radiology* **2014**, *271*, 688–694. [CrossRef] [PubMed]
23. Sun, Z. The promise of synchrotron radiation in medical science. *Australas. Med. J.* **2009**, *1*, 1–5. [CrossRef]
24. Sun, Z.; Ng, C.K.C.; Squelch, A. Synchrotron radiation computed tomography assessment of calcified plaques and coronary stenosis with different slice thicknesses and beam energies on 3D printed coronary models. *Quant. Imaging Med. Surg.* **2019**, *9*, 6–22. [CrossRef]
25. du Plessis, A.; Broeckhoven, C.; Guelpa, A.; le Roux, S.G. Laboratory x-ray micro-computed tomography: A user guideline for biological samples. *Gigascience* **2017**, *6*, gix027. [CrossRef]
26. Sun, Z.; Ng, C.K.C.; Wong, Y.H.; Yeong, C.H. 3D-printed coronary plaques to simulate high calcification in the coronary arteries for investigation of blooming artifacts. *Biomolecules* **2021**, *11*, 1307. [CrossRef]
27. Giannopoulos, A.A.; Steigner, M.L.; George, E.; Barile, M.; Hunsaker, A.R.; Rybicki, F.J.; Mitsouras, D. Cardiothoracic applications of 3-dimensional printing. *J. Thorac. Imaging* **2016**, *31*, 253–272. [CrossRef]
28. Lau, I.; Sun, Z. Dimensional accuracy and clinical value of 3D printed models in congenital heart disease: A systematic review and meta-analysis. *J. Clin. Med.* **2019**, *8*, 1483. [CrossRef]
29. Lee, S.; Squelch, A.; Sun, Z. Quantitative assessment of 3D printed model accuracy in delineating congenital heart disease. *Biomolecules* **2021**, *11*, 270. [CrossRef]
30. Valverde, I.; Gomez-Ciriza, G.; Hussain, T.; Suarez-Mejias, C.; Velasco-Forte, M.N.; Byrne, N.; Ordoñez, A.; Gonzalez-Calle, A.; Anderson, D.; Hazekamp, M.G.; et al. Three-dimensional printed models for surgical planning of complex congenital heart defects: An international multicentre study. *Eur. J. Cardio-Thorac. Surg.* **2017**, *52*, 1139–1148. [CrossRef]
31. Lau, I.W.W.; Liu, D.; Xu, L.; Fan, Z.; Sun, Z. Clinical value of patient-specific three-dimensional printing of congenital heart disease: Quantitative and qualitative assessments. *PLoS ONE* **2018**, *13*, e0194333. [CrossRef]
32. Sun, Z.; Wee, C. 3D printed models in cardiovascular disease: An exciting future to deliver personalized medicine. *Micromachines* **2022**, *13*, 1575. [CrossRef] [PubMed]
33. Sun, Z. Clinical applications of patient-specific 3D printed models in cardiovascular disease: Current status and future directions. *Biomolecules* **2020**, *10*, 1577. [CrossRef] [PubMed]

34. Sun, Z.; Wong, Y.H.; Yeong, C.H. Patient-specific 3D-printed low-cost models in medical education and clinical practice. *Micromachines* **2023**, *14*, 464. [CrossRef] [PubMed]

35. Mayer, R.; Liacouras, P.; Thomas, A.; Kang, M.; Lin, L.; Simonet, C.B., 2nd. 3D printer generated thorax phantom with mobile tumor for radiation dosimetry. *Rev. Sci. Instrum.* **2015**, *86*, 074301. [CrossRef] [PubMed]

36. Hou, K.Y.; Tsujioka, K.; Yang, C.C. Optimization of HU threshold for coronary artery calcium scans reconstructed at 0.5-mm slice thickness using iterative reconstruction. *J. Appl. Clin. Med. Phys.* **2020**, *21*, 111–120. [CrossRef]

37. Yang, Q.; Liu, J.; Barnes, S.R.; Wu, Z.; Li, K.; Neelavalli, J.; Hu, J.; Haacke, E.M. Imaging the vessel wall in major peripheral arteries using susceptibility-weighted Imaging. *J. Magn. Reason. Imaging* **2009**, *30*, 357–365. [CrossRef]

38. Suzuki, S.; Machida, H.; Tanaka, I.; Ueno, E. Vascular diameter measurement in CT angiography: Comparison of model-based iterative reconstruction and standard filtered back projection algorithms in vitro. *AJR Am. J. Roentgenol.* **2013**, *200*, 652–657. [CrossRef]

39. Sun, Z.; Ng, C.K.C. Synchrotron radiation imaging of aortic stent grafting: An in vitro phantom study. *J. Med. Imaging Health Inform.* **2017**, *7*, 890–896. [CrossRef]

40. Sun, Z.; Ng, C.K.C. Use of synchrotron radiation to accurately assess cross-sectional area reduction of the aortic branch ostia caused by suprarenal stent wires. *J. Endovasc. Ther.* **2017**, *24*, 870–879. [CrossRef]

41. Sun, Z.; Ng, C.K.C.; Sa Dos Reis, C. Synchrotron radiation computed tomography versus conventional computed tomography for assessment of four types of stent grafts used for endovascular treatment of thoracic and abdominal aortic aneurysms. *Quant. Imaging Med. Surg.* **2018**, *8*, 609–620. [CrossRef]

42. Kalisz, K.; Buethe, J.; Saboo, S.S.; Abbara, S.; Halliburton, S.; Rajiah, P. Artifacts at cardiac CT: Physics and solutions. *Radiographics* **2016**, *36*, 2064–2083. [CrossRef]

43. Xu, L.; Sun, Z. Virtual intravascular endoscopy visualization of calcified coronary plaques: A novel approach of identifying plaque features for more accurate assessment of coronary lumen stenosis. *Medicine* **2015**, *94*, e805. [CrossRef] [PubMed]

44. Sun, Z.; Dosari, S.A.; Ng, C.; al-Muntashari, A.; Almaliky, S. Multislice CT virtual intravascular endoscopy for assessing pulmonary embolisms: A pictorial review. *Korean J. Radiol.* **2010**, *11*, 222–230. [CrossRef]

45. Sun, Z.; Dimpudus, F.J.; Nugroho, J.; Adipranoto, J.D. CT virtual intravascular endoscopy assessment of coronary artery plaques: A preliminary study. *Eur. J. Radiol.* **2010**, *75*, e112–e119. [CrossRef] [PubMed]

46. Li, P.; Xu, L.; Yang, L.; Wang, R.; Hsieh, J.; Sun, Z.; Fan, Z.; Leipsic, J.A. Blooming artifact reduction in coronary artery calcification by a new de-blooming algorithm: Initial study. *Sci. Rep.* **2018**, *8*, 6945. [CrossRef] [PubMed]

47. Weir-McCall, J.R.; Wang, R.; Halankar, J.; Hsieh, J.; Hague, C.J.; Rosenblatt, S.; Fan, Z.; Sellers, S.L.; Murphy, D.T.; Blanke, P.; et al. Effect of a calcium deblooming algorithm on accuracy of coronary computed tomography angiography. *J. Cardiovasc. Comput. Tomogr.* **2020**, *14*, 131–136. [CrossRef] [PubMed]

48. Nikon Corporation. XT H 225 ST 2x. Available online: https://industry.nikon.com/en-aom//wp-content/uploads/sites/20/2022/12/xth-225-st-2x-en.pdf (accessed on 19 June 2023).

49. Leipsic, J.; Heilbron, B.G.; Hague, C. Iterative reconstruction for coronary CT angiography: Finding its way. *Int. J. Cardiovasc. Imaging* **2012**, *28*, 613–620. [CrossRef]

50. Wang, J.; Fleischmann, D. Improving spatial resolution at CT: Development, benefits, and pitfalls. *Radiology* **2018**, *289*, 261–262. [CrossRef]

51. Wu, S. The potential value of 320-row computed tomography angiography in digital subtraction angiography-Negative spontaneous subarachnoid hemorrhage patients. *J. Comput. Assist. Tomogr.* **2022**, *46*, 244–250. [CrossRef]

52. Trost, J.; Ferraro, R.; Sharma, G.; Hays, A.G.; Boden, W.E.; Blumenthal, R.S.; Arbab-Zadeh, A. CCTA should be the new diagnostic gateway for evaluating intermediate-risk stable angina patients. *JACC Adv.* **2022**, *1*, 100116. [CrossRef]

53. Kim, C.; Hong, S.J.; Ahn, C.M.; Kim, J.S.; Kim, B.K.; Ko, Y.G.; Choi, B.W.; Choi, D.; Jang, Y.; Hong, M.K. Clinical implications of moderate coronary stenosis on coronary computed tomography angiography in patients with stable angina. *Yonsei Med. J.* **2018**, *59*, 937–944. [CrossRef] [PubMed]

54. Koons, E.; VanMeter, P.; Rajendran, K.; Yu, L.; McCollough, C.; Leng, S. Improved quantification of coronary artery luminal stenosis in the presence of heavy calcifications using photon-counting detector CT. *Proc. SPIE Int. Soc. Opt. Eng.* **2022**, *12031*, 120311A. [CrossRef] [PubMed]

55. Zsarnoczay, E.; Fink, N.; Schoepf, U.J.; O'Doherty, J.; Allmendinger, T.; Hagenauer, J.; Wolf, E.V.; Griffith, J.P., 3rd; Maurovich-Horvat, P.; Varga-Szemes, A.; et al. Ultra-high resolution photon-counting coronary CT angiography improves coronary stenosis quantification over a wide range of heart rates-A dynamic phantom study. *Eur. J. Radiol.* **2023**, *161*, 110746. [CrossRef]

56. Si-Mohamed, S.A.; Boccalini, S.; Lacombe, H.; Diaw, A.; Varasteh, M.; Rodesch, P.A.; Dessouky, R.; Villien, M.; Tatard-Leitman, V.; Bochaton, T.; et al. Coronary CT angiography with photon-counting CT: First-in-human results. *Radiology* **2022**, *303*, 303–313. [CrossRef]

57. Hagar, M.T.; Soschynski, M.; Saffar, R.; Ran, A.; Taron, J.; Weiss, J.; Stein, T.; Faby, S.; von zur Mueblen, C.; Ruile, P.; et al. Accuracy of ultrahigh-resolution photon-counting CT for detecting coronary artery disease in a high-risk population. *Radiology* **2023**, *307*, e223305. [CrossRef]

58. Soschynski, M.; Hagen, F.; Baumann, S.; Hagar, M.T.; Weiss, J.; Krauss, T.; Schlett, C.L.; von zur Muhlen, C.; Nikolaou, K.; Greulich, S.; et al. High temporal resolution dual-source photon-counting CT for coronary artery disease: Initial multicenter clinical experience. *J. Clin. Med.* **2022**, *11*, 6003. [CrossRef]

59. Yang, J.; Shan, D.; Wang, X.; Sun, X.; Shao, M.; Wang, K.; Pan, Y.; Wang, Z.; Schoepf, U.J.; Savage, R.H.; et al. On-site computed tomography-derived fractional flow reserve to guide management of patients with stable coronary artery disease: The TARGET randomized trial. *Circulation* **2023**, *147*, 1369–1381. [CrossRef]

60. Douglas, P.S.; De Bruyne, B.; Pontone, G.; Patel, M.R.; Norgaard, B.L.; Byrne, R.A.; Curzen, N.; Purcell, I.; Gutberlet, M.; Rioufol, G.; et al. 1-year outcomes of FFRCT-guided care in patients with suspected coronary artery disease: The PLATFORM Study. *J. Am. Coll. Cardiol.* **2016**, *68*, 435–445. [CrossRef]

61. Curzen, N.; Nicholas, Z.; Stuart, B.; Wilding, S.; Hill, K.; Shambrook, J.; Eminton, Z.; Ball, D.; Barrett, C.; Johnson, L.; et al. Fractional flow reserve derived from computed tomography coronary angiography in the assessment and management of stable chest pain: The FORECAST randomized trial. *Eur. Heart J.* **2021**, *42*, 3844–3852. [CrossRef]

62. Gao, X.; Wang, R.; Sun, Z.; Zhang, H.; Bo, K.; Xue, X.; Yang, J.; Xu, L. A novel CT perfusion-based fractional flow reserve algorithms for detecting coronary artery disease. *J. Clin. Med.* **2023**, *12*, 2154. [CrossRef] [PubMed]